Shear Banding in Drying Films of Colloidal Nanoparticles

Bin Yang,[†] James S. Sharp,[†,‡] and Michael I. Smith[*,†]

[†]School of Physics and Astronomy and [‡]Nottingham Nanotechnology and Nanoscience Centre, University of Nottingham, University Park, Nottingham, NG7 2RD, United Kingdom

ABSTRACT Drying suspensions of colloidal nanoparticles exhibit a variety of interesting strain release mechanisms during film formation. These result in the selection of characteristic length scales during failure processes such as cracking and subsequent delamination. A wide range of materials (*e.g.*, bulk metallic glasses) release strain through plastic deformations which occur in a narrow band of material known as a shear band. Here we show that drying colloidal films also exhibit shear banding. Bands are observed to form a small distance behind the drying front and then to propagate rapidly at ∼45° to the direction of drying. It is shown that the spacing of the bands depends on salt concentration and the evaporation rate of the colloidal suspension. These combined observations suggest that there is a critical shear rate (related to the film yield stress) which controls the ratio of bandwidth to band spacing. Local deformations were measured in the early stages of drying using fluorescent tracer particles. The measurements were used to show that the existence of shear bands is linked to the compaction of particles perpendicular to the drying front. The spacing of shear bands was also found to be strongly correlated with the characteristic length scale of the compaction process. These combined studies elucidate the role of plastic deformation during pattern formation in drying films of colloidal nanoparticles.

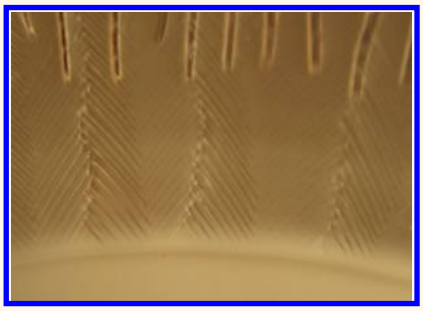

KEYWORDS: shear bands · film formation · colloid · nanoparticles · drying · plastic deformation · complex fluids

Shear banding, in which a material yields in strongly localized regions when subjected to an external stress, occurs in a wide range of materials such as metallic glasses,[1] granular materials,[2] complex fluids,[3−7] and glacial faults.[8] The formation and propagation of shear bands influence the material properties and often accompany failure mechanisms. Structures showing some similarity to the shear band patterns observed in metallic glasses have also recently been observed in drying films of colloidal nanoparticle suspensions.[9,10]

Thin film deposition, by the drying of suspensions of small particles (1−1000 nm), is a common technological process for the application of paints, inks, and glazes. The process of film formation results in a complex interaction between the liquid and particles. Initially, evaporation leads to the deposition of a few particles at the edge of a reservoir of particulate suspension. These particles result in the contact line becoming pinned.[11] Flows within the fluid then result in particles being swept to the drying edge, where a film is formed. As evaporation continues, the liquid retreats from the drying edge of the film, leading to the development of several distinct phases (Figure 1a): a reservoir of liquid suspension (i); a water-saturated film of close-packed particles (iii) and a largely dry film (not shown).

Recent studies have focused on the structural and dynamical changes that occur between these two regions (i and iii). Goehring *et al.*[12] showed that in this narrow region, "the transition region" (Figure 1a, region ii), the particles undergo irreversible aggregation into a network of particles in contact, which exhibits a finite yield stress. In the water-saturated film (region iii in Figure 1a), liquid is drawn through the porous film to the dry edge by capillary forces.[13] These forces can be substantial and place the entire film under stress (∼0.1−10 MPa).[14−16] This stress, combined with the constraint provided by the substrate,[16] can produce cracks which propagate through the film (Figure 1a region iii). Crack propagation in colloidal films is often studied, using elastic fracture mechanics ("the Griffith criterion"). However, recent work has highlighted the role

* Address correspondence to mike.i.smith@nottingham.ac.uk.

Received for review January 8, 2015 and accepted March 31, 2015.

Published online March 31, 2015
10.1021/acsnano.5b00127

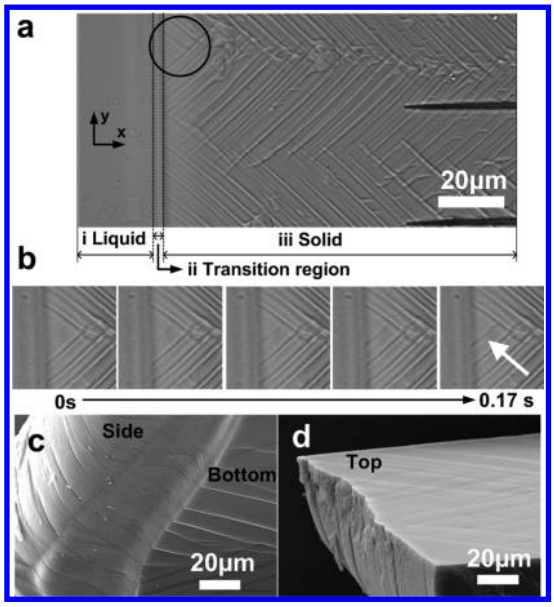

Figure 1. (a) Optical micrograph of a drying film of 50 nm polystyrene particles. Diagonal lines are observed to first form under the apex of chevrons and then propagate behind the transition region (ii). (b) Time lapse sequence of images showing the beginning of a shear band. (c,d) Scanning electron microscopy images of the bottom and top of a piece of colloidal film. The shear bands form vertical planes through the entire film.

of plastic deformations in the film near the crack tips, a significant distance behind the transition region (~1−2 mm).[17]

Under certain conditions, diagonal bands occur near the transition region and these are often oriented at ~45° to the direction of drying (Figure 1a). It has been proposed that these bands may arise from a buckling of the film surface due to capillary stresses.[10] An alternative suggestion is that these are shear bands,[9,10] an assertion which is based on the visual similarities that exist with structures commonly observed in both compressive and tensile tests on bulk metallic glasses. However, as yet, there is no direct evidence of the nature of these diagonal bands or an understanding of the processes responsible for their formation.

The focus of this study is on understanding the formation of these diagonal bands in drying colloidal films. Following a discussion of the characteristics of the bands formed, we examine the spacing and bandwidth in the light of some simple theories of shear banding. We conclude the paper by measuring the deformations associated with the early stages of film formation, showing that these are responsible for the band formation and spacing.

RESULTS AND DISCUSSION

Suspensions of charge-stabilized polystyrene (PS) nanoparticles (50, 100, and 200 nm) of different concentrations (~2.5−10 vol %) were spread on a glass substrate with the edge of a clean glass slide. The substrate was tilted at an angle ~4° to the horizontal, which resulted in a planar drying front which propagated from the raised edge toward the unraised edge. This resulted in a film being slowly formed at the raised edge, as the suspending liquid evaporated. The films show a gradual change in thickness (~40%) on length scales comparable to the dimensions of the glass substrate (25 mm) from top to bottom but vary little (<7%) parallel to the drying front.

Figure 1a illustrates a number of interesting observations concerning the formation and propagation of the diagonal bands formed in a drying colloidal film (region iii). The bands which form are in two orthogonal directions, resulting in chevrons where they meet. Two types of chevrons are observed: those which point away ("chevron") and those which point toward the transition region ("anti-chevrons"). Bands are formed near chevrons and terminate at anti-chevrons. When lines from neighboring chevrons meet (at an anti-chevron), they do not immediately terminate or combine as might be expected for two converging cracks but may cross each other and continue for a small distance. It is not clear what determines the starting positions (*i.e.*, *y* coordinates in Figure 1) of a new series of chevrons (there are no obvious film defects). The spacing of chevrons is much larger than other features of the film (*e.g.*, crack spacing), and while it is of a constant magnitude, it is somewhat variable even in a carefully controlled planar geometry.

Figure 1b shows the origin of a new band that occur near chevrons. The band appears to originate neither in the transition region nor from other shear bands but somewhere between. Careful observation of the new band shows that it forms when the gap between the transition region and the chevron apex reaches ~2λ (where λ is the band spacing). The band then grows rapidly ($\tau \sim 0.1$s) until it reaches the transition region and existing shear bands. Where a diagonal band already exists, it continues to propagate as the film dries, growing smoothly at the interface between regions ii and iii at an angle of approximately 45° to the transition region.

Once films are completely dry, small pieces are often observed to delaminate from the glass substrate, enabling the top, bottom, and side surfaces to be imaged. Figure 1c,d shows two scanning electron microscopy (SEM) images of a small piece of 50 nm PS colloidal film. Figure 1c shows the bottom and side surface of such a piece of film, while Figure 1d shows the same piece of film from the top. Top *and* bottom surfaces both show diagonal banding at 45° to the drying direction. Observation of the sides of the film shows that these bands are connected by a plane which runs vertically through the film. This would exclude surface buckling as the primary explanation for the diagonal bands which appear to occur as the result of a shift of one piece of the film relative to the other. This suggests that these structures are indeed

shear bands and that the banding is not the result of a surface buckling instability.

Behind the transition region, the film consists of a closely packed network of particles in contact.[12] Figure 1b shows that it is in this region that the shear bands appear to form. In metallic glasses, it is known that there exists an activation barrier for shear band nucleation.[18] Nucleation requires a localized dilatation of the sample, following which a shear band propagates rapidly.[18]

Observation of our samples also appears to show that the initial formation of shear bands is the key event in controlling both the development and subsequent spacing (Figure 1; also see discussion of Figure 3a). Because the plane of the bands, as discussed earlier, is vertical, this implies that the forces responsible for the banding are predominantly in the x direction (*i.e.*, in the plane of the film and perpendicular to the drying front).

Once band nucleation has occurred, the bands propagate at ~45° to the compression axis. This can be understood by determining the direction of the maximum resolved shear stress. If we consider a block of material with an axis parallel to the compression direction (see Supporting Information Figure S1), plastic deformations may occur along some plane, of area A, whose surface normal is at an angle ϕ to the compression axis. The projected area of this plane is $A/\cos\phi$. The compressive force F is spread over this plane and may be resolved into components normal to the plane and along the direction of maximum slope (indicated in Supporting Information Figure S1). However, the slip direction may not, in general, be the same as this. The slip direction occurs at an angle θ to the compression direction. The resolved shear stress can then be written as

$$\tau = (F/A)\cos\phi\cos\theta \quad (1)$$

By definition, as ϕ increases, θ decreases. This quantity therefore reaches a maximum when both ϕ and $\theta = 45°$. Hence plastic deformations are expected to occur at an angle of 45° to the compression axis.[19]

In our experiments, the bands were observed to occur in samples of 50 and 100 nm PS colloids but not for particle sizes of 200 nm or larger. Measurements of the band spacing (λ) show an approximately linear correlation with film thickness (H) in both cases, although the spacing in samples of 50 nm particles was considerably larger than that for the 100 nm particles (see Supporting Information Figure S2).

In order for a new band to form in a colloidal film through plastic deformation, the local stress applied to the particle network must exceed the shear yield stress of the film (τ_y). Although the concept of a true yield stress in colloidal systems has generated a large amount of discussion, it can be a helpful way of characterizing the properties of concentrated colloidal

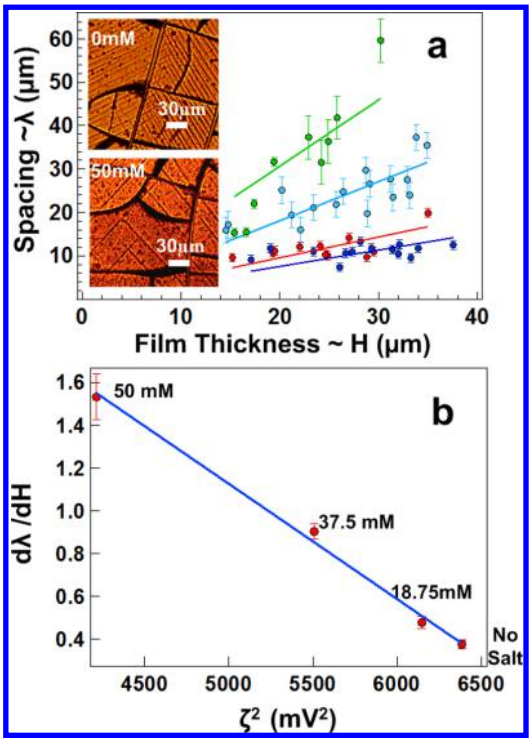

Figure 2. (a) Shear band spacing for different film thicknesses of 100 nm PS colloids containing 0 (dark blue), 18.75 (red), 37.5 (light blue), and 50 mM (green) added NaCl. Insets show typical optical micrographs of the dried films. The images show both cracks (vertical and horizontal lines) and shear bands (diagonal lines). (b) Plot of the fitted gradients from panel (a) for each salt concentration against the square of the measured ζ-potential (ζ^2).

suspensions.[20] The yield stress, τ_y, of strongly flocculated particles has been studied both theoretically[21] and experimentally[22,23] and shown to be linearly proportional to the square of the ζ-potential (ζ^2) with the functional form

$$\tau_y = A - B\zeta^2 \quad (2)$$

where A depends on the van der Waal's interactions and $B\zeta^2$ is the electrostatic contribution. Adding salt to colloidal solutions modifies the electrostatic interactions between particles and is therefore a relatively simple way of altering the yield stress in a colloidal film.

To test the dependence of the spacing of shear bands on the yield stress of the colloidal films, we performed experiments with different quantities of dissolved salt (0, 18.75, 37.5, and 50 mM NaCl) in solutions of 100 nm PS particles at ambient humidity and temperature. Figure 2a shows that the spacing of the bands increases linearly with the film thickness and that the addition of salt increases the slope of the curves. Taking the gradient of these curves gives us a measure of how the band spacing is altered by changing the concentration of the salt solutions. A Malvern Zetasizer was used to determine the ζ-potential of the particles at the different salt concentrations. The derivative of the band spacing ($d\lambda/dH$) was then plotted as

a function of the ζ-potential. Figure 2b shows that the band spacing depends on the square of the ζ-potential with the form

$$\frac{d\lambda}{dH} = a - b\zeta^2 \quad (3)$$

where a and b are constants. This is the same dependence which is known to exist for the yield stress. This is strong evidence that the formation and spacing of shear bands is dependent on the yield stress of the film.

Recent theoretical work on a minimal model of shear banding in thixotropic yield stress fluids has sought to understand shear banding in terms of the time scales for particle link breakage and formation.[24] This model predicts that there exists a critical shear rate ($\dot{\gamma}_c$) below which flows become unstable. It is argued that at shear rates immediately below $\dot{\gamma}_c$ the stress−strain rate curve has a negative gradient leading to an inherently unstable rheological behavior.[24,25] The existence of such a negative slope has been demonstrated for a strongly flocculated system of charged colloids using transient rheological measurements.[25] However, it is also possible to obtain shear banding when no negative gradient exists *via* shear−gradient concentration coupling.[26,27] Changes in local particle concentration may occur due to gradients in the shear rate. As the concentration in low shear rate regions increases, the shear gradients also increase, resulting in a self-amplifying process. This process also predicts that shear banding occurs below a critical shear rate $\dot{\gamma}_c$.

If shear banding is responsible for the observed diagonal bands, regardless of the mechanism, we expect a bifurcation into a region of elastic solid and a region of plasticity/flowing fluid (*i.e.*, shear banding). Experimentally, it has been confirmed that, in shear banding, the fraction of sheared material is determined by a ratio of the imposed shear rate to the critical shear rate (a material-dependent parameter).[25] If the imposed strain rate ($\dot{\gamma}_{dry}$) is important for the shear banding process in drying films, the fraction of sheared material should thus be given by a "Lever rule":[20,24]

$$\frac{\delta}{\lambda} \sim \frac{\dot{\gamma}_{dry}}{\dot{\gamma}_c} \quad (4)$$

where δ is the width of the sheared band and λ is the band spacing.

In a simple experiment, the evaporation rate of a drying sample of 100 nm particles was modified by covering the film with a glass dish (increasing the humidity near the film and reducing the evaporation rate). After the drying front had become established, the cover was removed. It was observed that the spacing between bands was significantly altered by changing the evaporation rate in this way (Figure 3a). Figure 3a also confirms that the spacing of bands is set by the initial formation of a band between the drying front and a chevron. This can be seen from the fact that

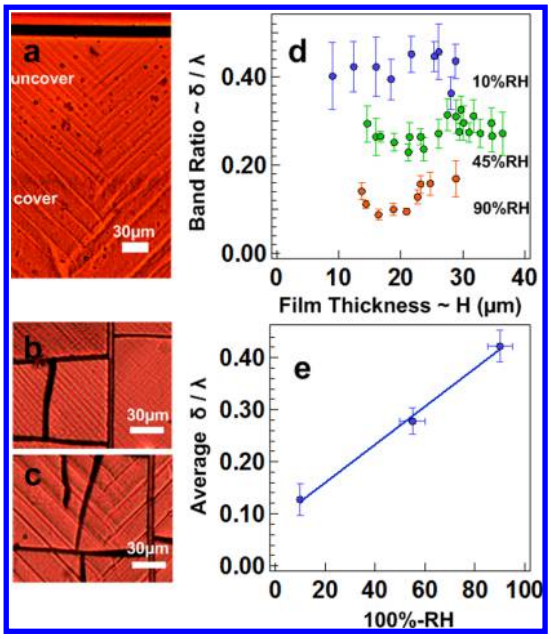

Figure 3. Effect of evaporation rate on shear band spacing in films of 100 nm PS particles. Example microscope images showing (a) how the shear band spacing changes when a film initially covered with a glass dish is uncovered, increasing the evaporation rate; (b) a film dried at a constant high evaporation rate; (c) a film dried at a constant low evaporation rate. The applicability of the Lever rule: (d) bandwidth (δ)/band spacing (λ) is independent of film thickness. (e) Average value of δ/λ scales linearly with the evaporation rate, which is proportional to 100% − RH.

the spacing between bands persists as they propagate into regions of different evaporation rate. However, newly created bands have a spacing set by the local evaporation rate. To control this process, we built a drying chamber in which the humidity was controlled by mixing various proportions of dry and moist air. Solutions were dried at measured relative humidities (RH) of 10 ± 5, 45 ± 5, and 90 ± 1% RH. In agreement with our earlier experiment, those experiments performed at low evaporation rates (high humidity) produced a much wider band spacing than those dried rapidly (Figure 3b,c).

The strain rate in a drying film is related to the velocity of the drying front. This is controlled by the evaporation of liquid from the reservoir of a colloidal suspension. For a fixed evaporation rate, this implies that $\dot{\gamma}_{dry}/\dot{\gamma}_c$ and hence δ/λ should be independent of film thickness. Although measurements of δ have a relatively large associated error, this agrees with the results presented in Figure 3d for all three evaporation rates. Due to the physical dimensions of the drying chamber (kept large to ensure the humidity was not influenced by the proximity of surfaces) and the working distance of the microscope objective, we could not measure the drying front velocity in our chamber directly. However, the evaporation rate $\dot{E}$ (which controls the drying front velocity) of a fluid at constant temperature is proportional to 100 − RH.[28] Making the

appropriate substitutions in eq 4, we arrive at the following scaling relation:

$$\frac{\delta}{\lambda} \propto \frac{\dot{E}}{\dot{E}_c} \propto \frac{(100 - \mathrm{RH})}{\dot{E}_c} \qquad (5)$$

where $\dot{E}_c$ is a critical evaporation rate. Figure 3e shows that the mean value of δ/λ increases approximately linearly with evaporation rate, as predicted by eq 5.

In our study of the effect of salt concentration on shear band spacing, samples were dried at constant humidity, leading to a constant evaporation rate. Varying the salt concentration was shown to modify the film yield stress. Coussot *et al.*[24] showed that an increase in the yield stress results in an increase of the critical shear rate $\dot{\gamma}_c$. Our earlier results, concerning the effect of salt concentration on the band spacing, may therefore be understood in terms of differences in the critical shear rate. Using the Lever rule, this predicts a decrease in the value of δ/λ with increasing salt concentration, which is what is observed.

This simple analysis using a Lever rule assumes a neat separation of the film into a static elastic component (between each band) and a plastically deforming band. Drying films cannot, however, be quite this simple because, as we show below, compaction of the film is occurring throughout a significant region behind the transition region. In this region, there are inevitably gradients in film properties in the *x* direction. Compaction also implies that the whole film is deforming and not simply the bands. It seems preferable, therefore, to think of the film as bifurcating into two regions with strongly differing degrees of flow. The essential principles, however, remain unchanged and confirm that our samples display the important features associated with shear banding.

We now turn to the question of the cause of shear band formation. Experiments were performed in which 1 μm fluorescent tracer particles were mixed at very low concentrations into suspensions of the nonfluorescent 50, 100, and 200 nm PS nanoparticles. At such low concentrations, there were no measurable differences in the shear bandwidth or spacing as a result of the large fluorescent particles. Using an upright microscope, we combined low-intensity transmission microscopy with fluorescent microscopy in reflection mode. When the relative intensities were adjusted, it was possible to visualize the film and its shear bands, while simultaneously observing the larger fluorescent particles (Figure 4a).

As fluorescent particles became trapped in the film at the first part of the transition region, their *x* and *y* coordinates (x_0,y_0) were determined within an accuracy of approximately ± 0.3 μm. The *y* coordinate in the lateral direction of each fluorescent particle was defined relative to the chevron center (+ to the left and − to the right; see Figure 4a). In subsequent frames, these coordinates (x,y) and their distance (D)

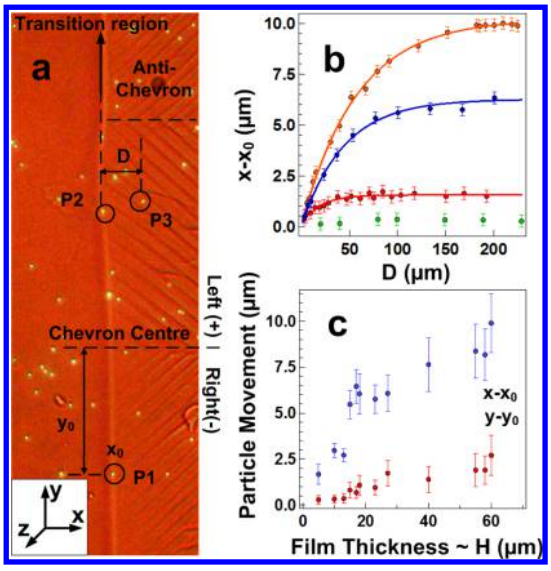

Figure 4. Measuring film deformations. (a) Microscope image of fluorescent particle tracking. Particle coordinates (x,y) are obtained relative to initial coordinates (x_0,y_0) in each frame. The distance from the particle to the beginning of the transition region (D) and the distance to the chevron center are also measured. (b) Example plots of the relative motion in the *x* direction of particles embedded in films of 200 nm (green), 100 nm (red), and 50 nm (blue and yellow) particles of film thicknesses 38 ± 5, 25 ± 5, 27 ± 5, and 60 ± 10 μm, respectively. (c) Total movement dx_{max} and dy_{max} in the *x* and *y* directions for films of 50 nm particles for different film thicknesses (H).

from the retreating edge of the transition region were remeasured (see Figure 4a). The tracking of particles showed that they were not completely static but moved a small distance relative to their initial coordinates. Figure 4b shows example plots of the relative position of particles ($dx = x - x_0$) perpendicular to the drying front as a function of D.

Tracking the movement of fluorescent particles embedded in the film enables us to infer how the film is deforming. The data in Figure 4b show example plots of particle tracking in films of 50, 100, and 200 nm particles. Samples of 50 and 100 nm particles show significant movement, while for samples of 200 nm particles, the displacements are negligible and certainly below the resolution of our experiment (see Supporting Information 3). We note that this difference in movement corresponds to the presence or absence of shear bands in the corresponding films. The motion of the fluorescent particles in the *x* direction (perpendicular to the transition region) for films of 50 and 100 nm particles can be fitted to a single exponential:

$$dx = dx_{max}[1 - \exp(-D/\lambda_{fit})] \qquad (6)$$

The magnitude of dx_{max} is a measure of the maximum amount of compaction in the *x* direction occurring in the film and is observed to be largest in films of 50 nm particles. We find that the decay lengths λ_{fit} of different data sets vary for different particle sizes

TABLE 1. Comparison of the Fitted Decay Length to Measured Shear Band Spacings

particle size (nm)	H (μm)	λ_{fit} (μm)	λ_{meas} (μm)
50	60 ± 10	58 ± 2	56 ± 10
50	27 ± 5	44 ± 3	38 ± 3
100	25 ± 5	19 ± 4	13 ± 2

(50 and 100 nm) and film thicknesses. However, in each case, the value of λ_{fit} is very close to, although consistently slightly larger than, the shear band spacing λ_{meas} measured from the corresponding images. For the example data sets shown in Figure 4b, this is summarized in Table 1.

This correspondence between the length scale of compaction and shear band spacing in x is strong evidence that it is compaction that causes the shear bands to form.

Figure 4c shows that the total amount of compaction dx_{max} is strongly dependent on the film thickness. This is also true of the associated decay length scale λ_{fit} (see Table 1 and Figure 4b), which would account for the change in the spacing of shear bands with increasing film thickness. While a critical shear rate can be used in conjunction with a Lever rule to explain the ratio δ/λ, it leaves unanswered the reasons for the system selecting a particular bandwidth δ or spacing λ. Arguments for specific bandwidths have been advanced in 2D granular systems based on purely geometrical considerations such as particle size.[29] Our measurements, which measure the movement of the upper surface, however, appear to indicate that it is the band spacing (λ) that is selected due to the process of compaction in the film. A no-slip boundary condition at the substrate would result in shear, as the top surface contracts relative to the substrate. The maximum strain relative to the substrate before yield would then be film-thickness-dependent. This mirrors arguments put forward for crack formation where substrate constraint is known to be important.[16] Compaction of the film following the transition region therefore plays a crucial role in determining, first, whether shear banding will occur and, second, setting the characteristic length scale responsible for the shear band spacing.

For the thickest 50 nm particle films, individual fluorescent particles which are at the surface of the film are observed to move in and out of focus as the film shrinks vertically. It is possible to estimate the height changes by adjusting the focus of the microscope as the particles move relative to the transition region. This crude approach indicates a total height change of $\sim 20 \pm 8\%$ for 50 nm particles. The height changes are pronounced at small values of D (*i.e.*, close to the transition region) and saturate over length scales similar to those measured in x.

For films of 50 nm particles where the motion of particles is large, we also observed that particles move a small distance in the y direction ($dy = y - y_0$). Plots of dy against D show a similar exponential movement; however, the magnitudes of displacement are considerably smaller while still above the accuracy of measurement (see Supporting Information 3). Particles located to the left of a chevron always move left, while those to the right move to the right, suggesting that this movement is linked to band formation. Figure 4c shows the average total movement (dx_{max} and dy_{max}) of $\sim$10 particles at a wide range of film thicknesses. There is an approximately constant ratio ($\sim 0.17 \pm 0.05$) between the total contraction in x and expansion in y. Some of the contraction in x and z *via* Poisson's ratio should result in expansion in the y direction. However, it is intriguing that this expansion is centered on the chevron's in the film. It seems unlikely that the whole film expands laterally since the film is effectively of infinite extent in this direction, and any movements must therefore be accommodated locally. Indeed, we find no correlation between the global y coordinate of the particle and the distance (dy) moved, implying that the deformations measured relate at least in part to the local movements of bands being formed. Observation of bands both in SEM and optical microscopy shows that there is a height change in the region of the band, implying that some material has been forced upward (z direction) by the plastic deformation of the film. It seems that the movements in y are therefore likely to be the result rather than the cause of the shear banding process.

To test the idea that movements in the y direction can be understood as arising from the movement of shear bands, we tracked particles which were located inside the chevron. Supporting Information movie 1 shows a particle tracked from the moment it crosses the transition region (the right-hand side of the movie shows a higher magnification image of the particle featured on the left). The particle initially travels in a straight line in the x direction due to compaction in the film and the absence of shear (red line). At a certain point, a shear band appears ahead of the particle, enabling the piece of film containing the particle to move laterally as the material in the band is sheared. This can be seen by the way the particle changes direction at the moment the shear band appears. It then continues to travel in this new direction with a small y component for some distance (blue line). It is reasonable to assume that a similar effect due to shear occurs in x; however, it is masked by the larger movements due to compaction. Although the resolution of our experiments prevents a more detailed analysis, this clearly demonstrates the shear motions present in a shear-banded film.

In summary, following the transition region if a film of colloidal nanoparticles undergoes sufficient compaction perpendicular to the drying front, shear bands are formed along the direction of maximum resolved

shear stress. The compaction process sets the length scale governing the spacing of these shear bands, which arise due to an instability inherent in colloidal yield stress materials. Below some critical strain rate (which depends on the yield stress of the material), this instability leads to a bifurcation into two bands. The relative fractions of material obey a simple Lever rule.

MATERIALS AND METHODS

Colloidal suspensions of PS nanoparticles (10% solids content, Varian) were diluted to different concentrations (~2.5−10 vol %) using deionized water. The sizes of the latex particles used were 50, 100, and 200 nm. The effect of ionic concentration was also studied using solutions of NaCl ranging from 0 to 50 mM. The particles were sonicated in sealed vials thoroughly before use to ensure complete dispersion.

Glass microscopy slides (25 mm × 25 mm) were cleaned sequentially by sonication using detergent, acetone, methanol, and deionized water before being dried with nitrogen gas.

Measurements of Shear Bands/Film Thickness. The local thickness of the dried colloidal films was determined in different locations on each sample using a Dektak profilometer (Veeco Instruments). Optical microscope images (Olympus BX51 with DP70 camera) of the dried colloidal films were then collected in transmission mode near the locations used for the film thickness measurements. The images were then analyzed using Image Pro Plus 4.0 image capture/analysis software (Media Cybernetics). For each image, five locations were chosen, and at each position, the spacing of 10 bands was manually measured. The values and uncertainties reported reflect the average and standard deviation of these measurements. High-magnification images were also collected with a 60× objective from which the shear bandwidths were measured. Each measurement was based on an average of 10 band measurements in the same region.

ζ-Potential Measurements. One hundred nanometer PS particles were diluted with solutions of 0, 18.75, 37.5, and 50 mM NaCl. A Zetasizer nano ZS from Malvern Instruments was used to measure the electrophoretic mobility and infer the ζ-potential. The ζ-potentials were calculated using the Henry function approximation[30] $f(\kappa a) \approx (16 + 18\kappa a + 3(\kappa a)^2)/(16 + 18\kappa a + 2(\kappa a)^2)$ with a being the particle radius and the calculated Debye length ($\kappa^{-1} = 0.304/(\mathrm{NaCl})^{1/2}$ nm).

SEM. SEM images were collected of small pieces of colloidal film coated with ~5 nm of platinum using a FEG-SEM (XL30 FEG ESEM).

Conflict of Interest: The authors declare no competing financial interest.

Acknowledgment. We thank N. Weston for help with the SEM imaging. M.S. gratefully acknowledges a Royal Society University Research Fellowship. Funding is acknowledged from EPSRC Grant EP/L003651/1.

Supporting Information Available: Diagram explaining the maximum resolved shear stress, additional experimental data comparing 50 and 100 nm particle sizes. Also included are further details of the particle tracking methodology, including a discussion of errors, and a movie showing the movement of a particle before and after shear band formation. This material is available free of charge *via* the Internet at http://pubs.acs.org.

REFERENCES AND NOTES

1. Schroers, J.; Johnson, W. L. Ductile Bulk Metallic Glass. *Phys. Rev. Lett.* **2004**, *93*, 255506.
2. Chichili, D. R.; Ramesh, K. T.; Hemker, K. J. Adiabatic Shear Localization in alpha-Titanium: Experiments, Modelling and Microstructural Evolution. *J. Mech. Phys. Solids* **2004**, *52*, 1889–1909.
3. Olmsted, P. D. Perspectives on Shear Banding in Complex Fluids. *Rheol. Acta* **2008**, *47*, 283–300.
4. Callaghan, P. T. Rheo NMR and Shear Banding. *Rheol. Acta* **2008**, *47*, 243–255.
5. Dhont, J. K. G.; Briels, W. J. Gradient and Vorticity Banding. *Rheol. Acta* **2008**, *47*, 257–281.
6. Manneville, S. Recent Experimental Probes of Shear Banding. *Rheol. Acta* **2008**, *47*, 301–318.
7. Fielding, S. M. Shear Banding in Soft Glassy Materials. *Rep. Prog. Phys.* **2014**, *77*, 102601.
8. Koehn, D.; Sachau, T. Two-Dimensional Numerical Modelling of Fracturing and Shear Band Development in Glacier Fronts. *J. Struct. Geol.* **2014**, *61*, 133–142.
9. Boulogne, F.; Pauchard, L.; Giorgiutti-Dauphine, F.; Botet, R.; Schweins, R.; Sztucki, M.; Li, J.; Cabane, B.; Goehring, L. Structural Anisotropy of Directionally Dried Colloids. *Europhys. Lett.* **2014**, *105*, 38005.
10. Berteloot, G.; Hoang, A.; Daerr, A.; Kavehpour, H. P.; Lequeux, F.; Limat, L. Evaporation of a Sessile Droplet: Inside the Coffee Stain. *J. Colloid Interface Sci.* **2012**, *370*, 155–161.
11. Deegan, R. D.; Bakajin, O.; Dupont, T. F.; Huber, G.; Nagel, S. R.; Witten, T. A. Capillary Flow as the Cause of Ring Stains from Dried Liquid Drops. *Nature* **1997**, *389*, 827–829.
12. Goehring, L.; Clegg, W. J.; Routh, A. F. Solidification and Ordering during Directional Drying of a Colloidal Dispersion. *Langmuir* **2010**, *26*, 9269–9275.
13. Dufresne, E. R.; Corwin, E. I.; Greenblatt, N. A.; Ashmore, J.; Wang, D. Y.; Dinsmore, A. D.; Cheng, J. X.; Xie, X. S.; Hutchinson, J. W.; Weitz, D. A. Flow and Fracture in Drying Nanoparticle Suspensions. *Phys. Rev. Lett.* **2003**, *91*, 224501.
14. Xu, Y.; Engl, W. C.; Jerison, E. R.; Wallenstein, K. J.; Hyland, C.; Wilen, L. A.; Dufresne, E. R. Imaging In-Plane and Normal Stresses near an Interface Crack Using Traction Force Microscopy. *Proc. Natl. Acad. Sci. U.S.A.* **2010**, *107*, 14964–14967.
15. Man, W. N.; Russel, W. B. Direct Measurements of Critical Stresses and Cracking in Thin Films of Colloid Dispersions. *Phys. Rev. Lett.* **2008**, *100*, 198302.
16. Smith, M. I.; Sharp, J. S. Effects of Substrate Constraint on Crack Pattern Formation in Thin Films of Colloidal Polystyrene Particles. *Langmuir* **2011**, *27*, 8009–8017.
17. Goehring, L.; Clegg, W. J.; Routh, A. F. Plasticity and Fracture in Drying Colloidal Films. *Phys. Rev. Lett.* **2013**, *110*, 024301.
18. Perepezko, J. H.; Imhoff, S. D.; Chen, M. W.; Wang, J. Q.; Gonzalez, S. Nucleation of Shear Bands in Amorphous Alloys. *Proc. Natl. Acad. Sci. U.S.A.* **2014**, *111*, 3938–3942.
19. Smallman, R. E.; Bishop, R. J. *Modern Physical Metallurgy and Materials Engineering*; Elsevier Science Ltd.: Amsterdam, 1999.
20. Møller, P. C. F.; Chikkadi, A.; Derks, V. D.; Bonn, D. An Attempt To Categorize Yield Stress Fluid Behaviour. *Philos. Trans. R. Soc., A* **2009**, *367*, 5139–5155.
21. Leong, Y. K.; Scales, P. J.; Healy, T. W.; Boger, D. V.; Buscall, R. Rheological Evidence of Adsorbate-Mediated Short-Range Steric Forces in Concentrated Dispersions. *J. Chem. Soc., Faraday Trans.* **1993**, *89*, 2473–2478.
22. Johnson, S. B.; Dixon, D. R.; Scales, P. J. The Electrokinetic and Shear Yield Stress Properties of Kaolinite in the Presence of Aluminium Ions. *Colloids Surf., A* **1999**, *146*, 281–291.
23. Scales, P. J.; Johnson, S. B.; Healy, T. W.; Kapur, P. C. Shear Yield Stress of Partially Flocculated Colloidal Suspensions. *AIChE J.* **1998**, *44*, 538–544.
24. Coussot, P.; Ovarlez, G. Physical Origin of Shear-Banding in Jammed Systems. *Eur. Phys. J. E* **2010**, *33*, 183–188.
25. Møller, P. C. F.; Rodts, S.; Michels, M. A. J.; Bonn, D. Shear Banding and Yield Stress in Soft Glassy Materials. *Phys. Rev. E* **2008**, *77*, 041507.

26. Besseling, R.; Isa, L.; Ballesta, P.; Petekedis, G.; Cates, M. E.; Poon, W. C. K. Shear Banding and Flow-Concentration Coupling in Colloidal Glasses. *Phys. Rev. Lett.* **2010**, *105*, 268301.
27. Jin, H.; Kang, K.; Ahn, K. H.; Dhont, J. K. G. Flow Instability Due to Coupling of Shear-Gradients with Concentration: Non-uniform Flow of (Hard-Sphere) Glasses. *Soft Matter* **2014**, *10*, 9470–9485.
28. Hammond, P.; Goslin, R. The Effect of Humidity Upon the Rate of Evaporation. *Ecology* **1933**, *14*, 411.
29. Francois, B.; Lacombe, F.; Herrmann, H. Finite Width of Shear Zones. *Phys. Rev. E* **2002**, *65*, 031311.
30. Swan, J. W.; Furst, E. M. A Simpler Expression for Henry's Function Describing the Electrophoretic Mobility of Spherical Colloids. *J. Colloid Interface Sci.* **2012**, *388*, 92–94.